APL Photonics

RESEARCH ARTICLE | SEPTEMBER 21 2023

Shaping single photons through multimode optical fibers using mechanical perturbations

Ronen Shekel ; Ohad Lib ; Rodrigo Gutiérrez-Cuevas ; Sébastien M. Popoff ; Alexander Ling; Yaron Bromberg

APL Photonics 8, 096109 (2023)
https://doi.org/10.1063/5.0161654

Shaping single photons through multimode optical fibers using mechanical perturbations

Cite as: APL Photon. 8, 096109 (2023); doi: 10.1063/5.0161654
Submitted: 11 June 2023 • Accepted: 23 August 2023 •
Published Online: 21 September 2023

Ronen Shekel,[1] Ohad Lib,[1] Rodrigo Gutiérrez-Cuevas,[2] Sébastien M. Popoff,[2] Alexander Ling,[3,4] and Yaron Bromberg[1,a)]

AFFILIATIONS

[1] Racah Institute of Physics, The Hebrew University of Jerusalem, Jerusalem 91904, Israel
[2] Institut Langevin, CNRS UMR 7587, ESPCI Paris, PSL Research University, 1 rue Jussieu, 75005 Paris, France
[3] Centre for Quantum Technologies, National University of Singapore, 3 Science Drive 2, 117543 Singapore
[4] Department of Physics, Faculty of Science, National University of Singapore, 2 Science Drive 3, 117551 Singapore

[a)] **Author to whom correspondence should be addressed:** yaron.bromberg@mail.huji.ac.il

ABSTRACT

Multimode optical fibers support low-loss transmission of multiple spatial modes, allowing for the transport of high-dimensional, spatially encoded information. In particular, encoding quantum information in the transverse shape of photons may boost the capacity of quantum channels while using existing infrastructure. However, when photons propagate through a multimode fiber, their transverse shape gets scrambled because of mode mixing and modal interference. This is usually corrected using free-space spatial light modulators, inhibiting a robust all-fiber operation. In this work, we demonstrate an all-fiber approach for controlling the shape of single photons and the spatial correlations between entangled photon pairs, using carefully controlled mechanical perturbations of the fiber. We optimize these perturbations to localize the spatial distribution of a single photon or the spatial correlations of photon pairs in a single spot, enhancing the signal in the optimized spot by over an order of magnitude. Using the same approach, we show a similar enhancement for coupling light from a multimode fiber into a single-mode fiber.

I. INTRODUCTION

Quantum technologies are revolutionizing the fields of communication,[1] sensing,[2] and computing.[3] Due to their low decoherence, photons are excellent candidates for transmitting quantum information between distant points and are often referred to as "flying qubits."[4,5] Photons also enjoy the advantage of existing mature optical fiber infrastructure offering low-loss transmission. In particular, multimode fibers (MMFs) can greatly boost the information capacity for both classical[6,7] and quantum[8–10] channels, by encoding high-dimensional information in the transverse shape of the photons. In the quantum regime, single photons have been delivered through MMFs for high-dimensional quantum key distribution (QKD)[11] and to increase the collection efficiency of free-space QKD.[12] In addition, photon pairs have been sent through the same MMF for creating programmable and high-dimensional quantum circuits.[13–15]

However, when classical or quantum light propagates through a complex medium, such as an MMF, the information it carries is scrambled due to the random interference between the different modes of the MMF. In particular, the spatial distribution of a single photon in a superposition of multiple fiber modes exhibits a speckle pattern at the output facet, exactly like classical coherent light, as depicted in Fig. 1. When pairs of spatially entangled photons propagate through MMFs, the spatial distribution of the intensity at the output of the fiber is uniform, yet the two-photon spatial correlations exhibit a speckle pattern, coined two-photon speckle. Given one photon arrives at a specific location, the spatial distribution of its twin exhibits the shape of a speckle pattern.[16–18]

The speckle and two-photon speckle patterns can be refocused to a spot by tailoring the wavefront at the input of the fiber using a spatial light modulator (SLM).[19–26] The wavefront can be found by measuring the transmission matrix of the fiber, from which the desired input is calculated,[27] or by using a "blind" optimization

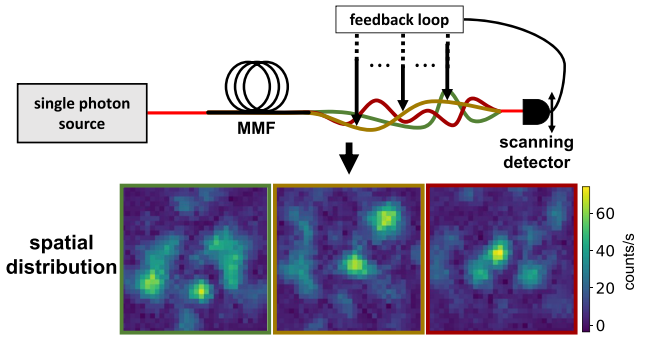

FIG. 1. When a photon propagates through a multimode fiber, its spatial distribution is scrambled, producing a speckle pattern. This speckle is highly sensitive to mechanical perturbations of the fiber, so different mechanical fiber conformations produce different output patterns. By optimizing controlled mechanical perturbations of the fiber, we localize the spatial distribution at the output.

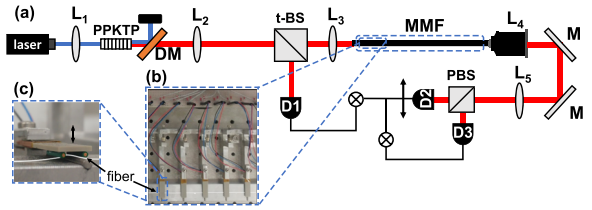

FIG. 2. Experimental setup. A continuous-wave pump laser (λ_p = 403.8 nm) is focused using a lens (L_1) upon a 4 mm periodically poled potassium titanyl phosphate (PPKTP) crystal, generating vertically polarized photon pairs via type-0 SPDC.[34] The pump beam is discarded using a dichroic mirror (DM), and the photon pairs are imaged through lenses L_2 and L_3 to the input facet of a graded index MMF. Along the MMF, 37 piezoelectric actuators are placed (b), inducing three-point local bends on the fiber (c). The output facet of the MMF is then imaged through lenses L_4 and L_5 to the coincidence measurement plane, where there are two single-photon detectors. The photons are split using a polarizing beam splitter (PBS), so one photon reaches a fixed detector (D_3) and the other reaches a scanning detector (D_2). In the heralded single-photon configuration, we place before the fiber a beam splitter with a tunable reflectivity, implemented by a $\frac{\lambda}{2}$ waveplate and a PBS. The PBS probabilistically routes one photon to the heralding detector (D_1) and the other photon into the fiber, where it is measured at its output by the scanning detector (D_2) (M—mirror; t-BS—tunable beam splitter).

scheme to maximize the signal at the focal spot.[28] Both methods rely on manipulating light outside the fiber, requiring careful alignment of the shaped wavefront into the fiber, thus inhibiting a robust all-fiber operation.

Recently, we have demonstrated an all-fiber approach for shaping classical light through MMFs. The transmission matrix of an MMF is highly sensitive to mechanical perturbations of the fiber,[29] as depicted in Fig. 1. Turning this nuisance into a feature, we have recently shown that by carefully applying controlled mechanical perturbations to the fiber, we could shape classical light in both the spatial[30] and spectral[31] domains, with no need for free-space propagation. The same concept has also been used to tailor nonlinear processes in MMFs.[32] We refer to this system of mechanical perturbations along the fiber as the *fiber piano*.

In this work, we use the fiber piano to refocus the spatial distribution of a single photon and the spatial correlations of photon pairs that propagate through an MMF. In both cases, we achieve over an order of magnitude enhancement of the signal in the focal spot. We further demonstrate the ability to enhance the coupling of a single photon from an MMF into a single-mode fiber (SMF), which could potentially increase the collection efficiency in free-space quantum communications.[12,33] These results pave the way for an all-fiber control of single photons and photon pairs through MMFs. With sufficient control over the photons and suppression of their scrambling, high-dimensional spatial encoding could be applied in quantum communications through MMFs, enhancing the capacity of quantum channels.

II. RESULTS

To demonstrate our all-fiber approach for shaping photons, we place 37 piezoelectric actuators along a graded index MMF with a core diameter of 50 μm. Each actuator creates a three-point contact that induces a local bend, as depicted in Fig. 2. We couple into the MMF photons generated by type-0 spontaneous parametric down-conversion (SPDC) (see Sec. IV). To study the shaping of a single photon passing through the MMF, we utilize the SPDC light to generate heralded single photons: we use a tunable beam splitter in front of the MMF to probabilistically route one of the photons to a heralding detector [D1 in Fig. 2(a)] and its twin photon to the MMF. Measuring the photon before the MMF informs us of the existence of the single photon state entering the MMF. We refer to this configuration as the heralded single photon configuration. The image plane of the output facet of the MMF is then scanned by a second detector (D2). The coincidence events between the two detectors, i.e., simultaneous detection of a photon by each of the detectors, reveal the spatial distribution of the heralded photon that passes through the MMF.

To study the correlations between pairs of photons that propagate together through the MMF, we tune the beam splitter before the fiber to couple both photons into the MMF. We refer to this configuration as the two-photon configuration. We place two detectors (D2 and D3) at the image plane of the MMF output facet. One detector is fixed in place, while the other scans the transverse plane, and the coincidence map reveals the two-photon spatial correlations. In both configurations, the collection of light to the detectors is performed using fibers with a core diameter of 50 μm, which is slightly smaller than the size of a single speckle grain. Narrowband filters and a polarizing beam splitter are placed before the detectors to ensure the detection of approximately a single polarization and spectral mode. For full details, see Sec. IV and the supplementary material.

As depicted in Fig. 3, when either a single heralded photon (a) or photon pairs (f) propagate through the MMF, the coincidence maps exhibit a speckle pattern [(b) and (g), respectively]. The total number of detected photons per pixel, known as the single counts, is equivalent to the classical intensity. It also exhibits a speckle pattern, yet with a low contrast [(c) and (h), respectively]. The reason for the low contrast in the single counts is that the two-photon quantum state we generate is in a superposition of ≈15 spatial modes that sum incoherently.[17] For a detailed discussion on the contrast of the single counts and on the number of modes in the system, see the supplementary material.

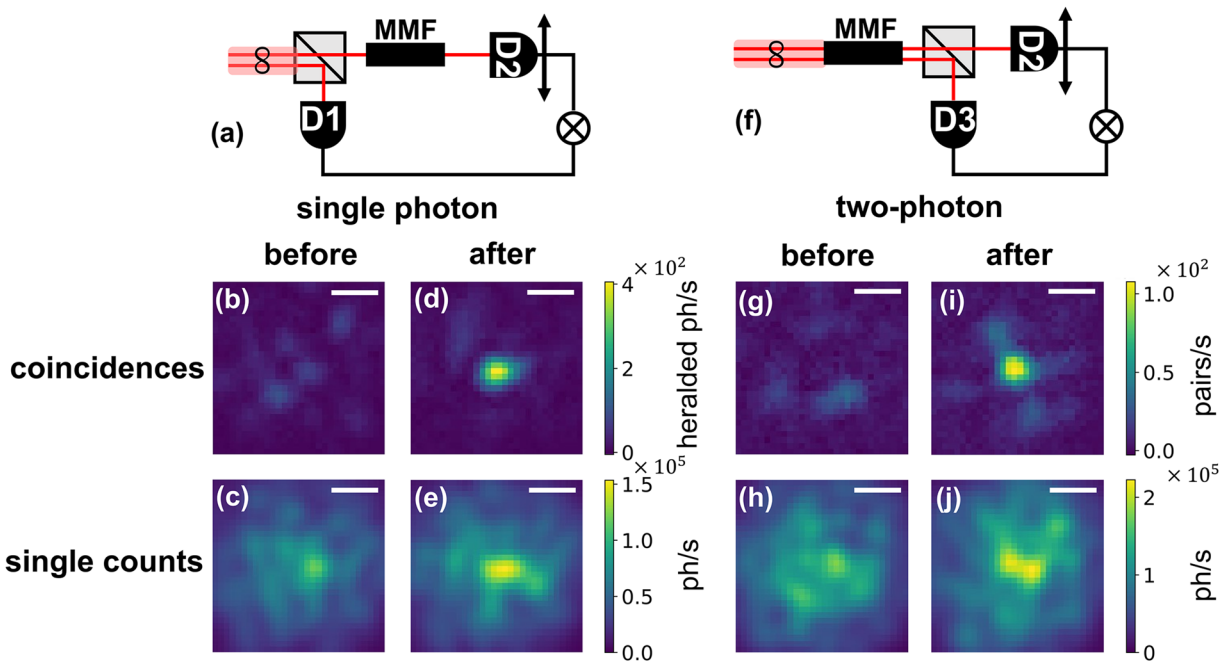

FIG. 3. We optimize the coincidence counts of single heralded photons [(a)–(e)] and photon pairs [(f)–(j)] passing through an MMF. Before the optimization process, the coincidence maps exhibit a speckle pattern [(b) and (g)]. After the optimization, the coincidence maps are strongly localized [(d) and (i)], with an enhancement factor of 16 ± 3 and 12 ± 2 for the one photon and two-photon configurations, respectively. As expected, the single counts [(c), (e), (h), and (j)] exhibit a low contrast and show only a slight enhancement compared with the coincidences. The collection of light to the detectors is performed using fibers with a core diameter of 50 μm, which is slightly smaller than the size of a single speckle grain. All scale bars represent 200 μm (ph—photons).

To refocus the spatial distribution of the heralded single photons and the spatial correlations of the photon pairs, we use a standard particle swarm optimization algorithm (chosen for ease of implementation) to find a set of mechanical perturbations that maximizes the coincidence rate of the two detectors, i.e., the rate of coincidence events, measured in counts per second. We define the enhancement as the ratio of the peak coincidence rate after optimization to the disorder average of the coincidence counts rate without optimization, when the collection fibers are at the same set locations. For the single photon experiment, we obtain an enhancement factor of 16 ± 3, and for the two-photon experiment, using the same optimization algorithm, we get an enhancement of 12 ± 2, as depicted in Figs. 3(d) and 3(i), respectively.

We note that optimization of the coincidence rate at the target position slightly enhances also the single counts at that position [Figs. 3(e) and 3(j)], yet by a factor ten times smaller. The small enhancement in the single counts shows that most of the enhancement of the correlations between the photons stems from unscrambling of the two-photon speckle pattern. The reason for this is that the two-photon signal is coherent, allowing us to set the relative phases of different modes to interfere constructively at a desired spot. This is in contrast to the incoherent case of the single counts where the relative phases cannot be kept fixed. A detailed discussion on the contributions of the single counts, the polarization, and the loss to the enhancement is given in the supplementary material.

Next, to demonstrate the flexibility of our approach to tailoring the shape of single photons and two-photon correlations, we perform the optimization to focus the coincidence maps on two spots. We optimize the coincidence counts between the fixed detector and each one of the two spots, simultaneously (see Sec. IV). Relative to the average coincidence counts at each spot, we achieve an enhancement of 4.1 ± 0.4 (4.7 ± 0.5) on the upper spot and 5.7 ± 0.5 (6.4 ± 0.8) on the lower spot in the single photon (two-photon) setting. The coincidence maps after the optimization process are shown in Fig. 4.

Finally, we consider the coupling of single photons from an MMF into an SMF. While sending single photons through MMFs is appealing when the information is encoded in the spatial degree of freedom, SMFs are more attractive in the case of temporal and polarization encoding. This is due to their lower dispersion and polarization mixing, better interface with superconducting detectors, and better components and infrastructure. However, in applications such as free-space quantum communications,[35,36] coupling into SMFs limits the link efficiency due to the need to map the distorted incoming wavefront to the single mode of the fiber. To demonstrate funneling of single photons through the MMF and coupling into an SMF, we couple heralded single photons into the MMF and then optimize the coupling efficiency into a single polarization mode of an SMF using mechanical perturbations. We show that after optimization, the collection efficiency into the SMF is enhanced by a factor of 11.3 ± 0.6. We show the optimiza-

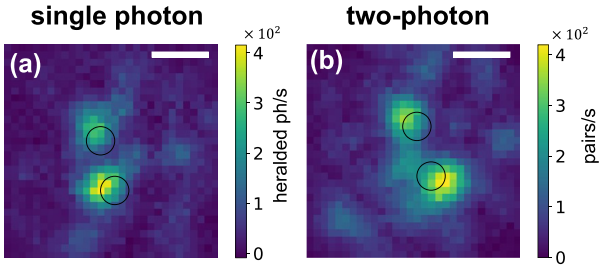

FIG. 4. To demonstrate a higher degree of control using mechanical perturbations, we change the cost function to optimize the coincidence counts between the fixed detector and each of two spots. This is performed both in the single photon configuration (a) and in the two-photon configuration (b). The collection of light to the detectors is performed using fibers with a core diameter of 100 μm, which is on the order of a single speckle grain. The locations of the collection fibers are indicated by the black circles. The two scale bars represent 200 μm (ph—photons).

tion process for the coupling into the SMF in the supplementary material.

III. DISCUSSION

We demonstrate the shaping of heralded single photons and photon pairs through MMFs via controlled mechanical perturbations, enhancing the signal at a focal spot by over an order of magnitude. The standard approach of shaping photons is by using SLMs, which exhibit low loss and have simple linear input–output relations that enable straightforward optimization. In comparison, the relationship between the actuator input voltages and the output field is non-linear and quite non-trivial as the perturbations are applied at different locations along the fiber. These non-trivial relations call for non-linear optimization methods, which are computationally harder. The main advantage of the fiber piano is that it is all-fiber, which can potentially offer a low-cost, low-loss, and robust solution upon further development.[32] Most importantly, all-fiber shaping eliminates the need to achieve precise coupling of a large number of modes encoding the information of the quantum state into an MMF, which is particularly challenging in the high-dimensional case.

Building on our demonstration of all-fiber shaping, we believe that utilizing recent demonstrations of the generation and detection of spatially entangled photons directly inside MMFs[37,38] could enable all-fiber implementations of high-dimensional quantum technologies. For example, the control of single photon propagation through MMFs could enable all-fiber high-dimensional QKD and entanglement distribution,[8,39] while the control of photon pairs propagating through the same MMF could enable all-fiber linear quantum networks.[14]

Another advantage of the fiber piano is that it allows tailoring of the entire transmission matrix of an MMF that supports N guided modes, by increasing the number of controlled actuators in the experiment to approximately N^2, which could be feasible in a few-mode fiber. This is in contrast to the degree of control that can be achieved with an SLM in front of the fiber, which can only control $2N$ degrees of freedom, namely the complex amplitudes of the excited guided modes. Therefore, we believe that scaling up our proof-of-concept demonstration will not only yield larger enhancements[30] but also provide an all-fiber approach for programming arbitrary transformations on multiple input modes. This is analogous to the advantage of using multiplane light converters (MPLCs) with respect to a single SLM in both classical[40–43] and quantum[44–46] experiments. We thus expect that while in this work our objective was to restore the correlations between specific modes, increasing the number of controlled actuators will allow for future applications in high-dimensional entanglement certification through MMFs[8,13,39] and for the realization of programmable linear quantum networks.[14]

Finally, similar to adaptive optics with deformable mirrors, which also rely on mechanical perturbations, we expect the optimization rate of our approach to be significantly improved by using a beacon laser for optimization,[13,24] fast electronics, and faster actuators, as discussed in the supplementary material. We thus believe that our demonstration could be relevant to improving the link efficiency in free-space quantum communications through turbulence.[47–49] This could be achieved by first coupling the distorted single photons into an MMF and then using mechanical perturbations to counter-effect the scattering in both the link and the MMF, yielding efficient coupling of the photons into an SMF.

IV. METHODS

The experimental setup is presented in Fig. 2. An $L = 4$ mm long PPKTP crystal is pumped by a continuous-wave laser (140 mW, $\lambda_p = 403.8$ nm). The wavefront of the pump beam is focused on the crystal using a lens with a focal length of $L_1 = 200$ mm. The pump profile in the crystal plane is approximately Gaussian with a waist of $w_0 \approx 110$ μm. The pairs of vertically polarized photons centered at $\lambda \approx 807.6$ nm are generated by the type-0 SPDC process.[34] Since the divergence of the pump beam (λ_p/w_0) is substantially smaller than the divergence of the emitted pairs $(\sqrt{\lambda/L})$, the pairs are generated in an entangled superposition of multiple transverse modes.[50] The pump beam is separated from the entangled photons using a dichroic mirror and sent to a beam dump. The entangled photons are then imaged through two lenses with focal lengths $L_2 = 200$ mm and $L_3 = 60$ mm to the facet of an ≈1.8 m long multimode bare fiber (Corning ClearCurve OM2, graded index, numerical aperture of 0.2, and core diameter of 50 μm). Between these lenses, the photons propagate through a $\lambda/2$ waveplate and a polarizing beam splitter (PBS), used for switching between the single photon and the two-photon configurations.

Along the fiber, we place 37 piezoelectric actuators (CTS NAC2225-A01), with a 3 cm separation between adjacent actuators, creating three-point contacts that induce local bends along the fiber. The range of curvatures induced by the bends was chosen such that they would induce a significant change in the speckle pattern while causing a relatively low loss of a few percent per actuator.

The far end of the fiber is imaged through a 20× objective lens (Olympus RMS20×) and another lens with focal length $L_5 = 300$ mm, through another PBS, to the coincidence measurement plane. The coincidence measurements are performed after passing through 3 nm FWHM bandpass filters (Semrock LL01-808-12.5), using 50 μm multimode fibers (Thorlabs FG050LGA, step

index, numerical aperture of 0.22) coupled to single photon detectors (Excelitas SPCM-AQRH). The coincidence counts are measured using a time tagger (Swabian, Time tagger 20), with a coincidence window of 1 ns. All coincidence counts shown in this paper are after subtracting the accidental counts.

In the single photon configuration, the heralding photon is collected between L2 and L3, using a 50 μm multimode fiber (Thorlabs FG050LGA). When we optimize for two spots, we use two fibers out of a fiber bundle with three 100 μm diameter cores, with a 200 μm separation between core centers (FiberTech Optica FTO-CTFOLA). In the two-photon configuration, when optimizing for two spots, we used also for the second fiber a 100 μm multimode fiber. To enhance the coincidence rates at the two spots, c_1 and c_2, such that $c_1 \approx c_2$, we maximize the cost function $\sqrt{c_1} + \sqrt{c_2} - \alpha \cdot |c_1 - c_2|$, where $\alpha \approx 0.04$ was adjusted to balance the trade-off between a high signal and an equal signal at both spots.

When coupling heralded single photons from an MMF into an SMF, we connect the fibers using a standard connector and further pass the photons through an inline fiber polarizer (Thorlabs ILP780PM-FC) before arriving at the detectors.

SUPPLEMENTARY MATERIAL

See the supplementary material for a detailed analysis of the spatial, spectral, and polarization modes in the system, as well as further details regarding the optimization process.

ACKNOWLEDGMENTS

This research was supported by the Zuckerman STEM Leadership Program and the ISF-NRF Singapore joint research program (Grant No. 3538/20). O.L. acknowledges the support of the Clore Scholars Programme of the Clore Israel Foundation. S.M.P. and R.G.-C. acknowledge the support of the French Agence Nationale pour la Recherche (Grant No. ANR-20-CE24-0016 MUPHTA) and Labex WIFI (Grant Nos. ANR-10-LABX-24 and ANR-10-IDEX-0001-02 PSL*).

AUTHOR DECLARATIONS

Conflict of Interest

The authors have no conflicts to disclose.

Author Contributions

Ronen Shekel: Conceptualization (equal); Formal analysis (equal); Investigation (equal); Methodology (equal); Software (equal); Validation (equal); Visualization (equal); Writing – original draft (equal); Writing – review & editing (equal). **Ohad Lib**: Formal analysis (equal); Investigation (equal); Writing – original draft (equal); Writing – review & editing (equal). **Rodrigo Gutiérrez-Cuevas**: Methodology (equal); Validation (equal); Writing – review & editing (equal). **Sébastien M. Popoff**: Conceptualization (supporting); Funding acquisition (supporting); Methodology (equal); Validation (equal); Writing – review & editing (equal). **Alexander Ling**: Conceptualization (equal); Funding acquisition (supporting); Writing – review & editing (equal). **Yaron Bromberg**: Conceptualization (equal); Funding acquisition (lead); Supervision (lead); Writing – review & editing (equal).

DATA AVAILABILITY

The data that support the findings of this study are available from the corresponding author upon reasonable request.

REFERENCES

[1] J. S. Sidhu, S. K. Joshi, M. Gündoğan, T. Brougham, D. Lowndes, L. Mazzarella, M. Krutzik, S. Mohapatra, D. Dequal, G. Vallone *et al.*, "Advances in space quantum communications," IET Quantum Commun. **2**, 182–217 (2021).
[2] E. Polino, M. Valeri, N. Spagnolo, and F. Sciarrino, "Photonic quantum metrology," AVS Quantum Sci. **2**, 024703 (2020).
[3] M. A. Nielsen and I. Chuang, *Quantum Computation and Quantum Information* (2002).
[4] D. P. DiVincenzo, "The physical implementation of quantum computation," Fortschr. Phys. **48**, 771–783 (2000).
[5] F. Flamini, N. Spagnolo, and F. Sciarrino, "Photonic quantum information processing: A review," Rep. Prog. Phys. **82**, 016001 (2018).
[6] B. J. Puttnam, G. Rademacher, and R. S. Luís, "Space-division multiplexing for optical fiber communications," Optica **8**, 1186–1203 (2021).
[7] Z. Ma, P. Kristensen, and S. Ramachandran, "Scaling information pathways in optical fibers by topological confinement," Science **380**, 278–282 (2023).
[8] N. H. Valencia, S. Goel, W. McCutcheon, H. Defienne, and M. Malik, "Unscrambling entanglement through a complex medium," Nat. Phys. **16**, 1112–1116 (2020).
[9] L. V. Amitonova, T. B. H. Tentrup, I. M. Vellekoop, and P. W. H. Pinkse, "Quantum key establishment via a multimode fiber," Opt. Express **28**, 5965–5981 (2020).
[10] Y. Zhou, B. Braverman, A. Fyffe, R. Zhang, J. Zhao, A. E. Willner, Z. Shi, and R. W. Boyd, "High-fidelity spatial mode transmission through a 1-km-long multimode fiber via vectorial time reversal," Nat. Commun. **12**, 1866 (2021).
[11] Y. Ding, D. Bacco, K. Dalgaard, X. Cai, X. Zhou, K. Rottwitt, and L. K. Oxenløwe, "High-dimensional quantum key distribution based on multicore fiber using silicon photonic integrated circuits," npj Quantum Inf. **3**, 25 (2017).
[12] J. Jin, S. Agne, J.-P. Bourgoin, Y. Zhang, N. Lütkenhaus, and T. Jennewein, "Demonstration of analyzers for multimode photonic time-bin qubits," Phys. Rev. A **97**, 043847 (2018).
[13] H. Defienne, M. Barbieri, I. A. Walmsley, B. J. Smith, and S. Gigan, "Two-photon quantum walk in a multimode fiber," Sci. Adv. **2**, e1501054 (2016).
[14] S. Leedumrongwatthanakun, L. Innocenti, H. Defienne, T. Juffmann, A. Ferraro, M. Paternostro, and S. Gigan, "Programmable linear quantum networks with a multimode fibre," Nat. Photonics **14**, 139–142 (2020).
[15] A. Makowski, M. Dąbrowski, I. M. Antolovic, C. Bruschini, H. Defienne, E. Charbon, R. Lapkiewicz, and S. Gigan, "Large reconfigurable quantum circuits with SPAD arrays and multimode fibers," arXiv:2305.16206 [quant-ph] (2023).
[16] C. Beenakker, J. Venderbos, and M. Van Exter, "Two-photon speckle as a probe of multi-dimensional entanglement," Phys. Rev. Lett. **102**, 193601 (2009).
[17] W. Peeters, J. Moerman, and M. Van Exter, "Observation of two-photon speckle patterns," Phys. Rev. Lett. **104**, 173601 (2010).
[18] H. Di Lorenzo Pires, J. Woudenberg, and M. Van Exter, "Statistical properties of two-photon speckles," Phys. Rev. A **85**, 033807 (2012).
[19] J. Carpenter, B. J. Eggleton, and J. Schröder, "110x110 optical mode transfer matrix inversion," Opt. Express **22**, 96–101 (2014).
[20] M. Plöschner, T. Tyc, and T. Čižmár, "Seeing through chaos in multimode fibres," Nat. Photonics **9**, 529–535 (2015).
[21] H. Defienne, M. Barbieri, B. Chalopin, B. Chatel, I. Walmsley, B. Smith, and S. Gigan, "Nonclassical light manipulation in a multiple-scattering medium," Opt. Lett. **39**, 6090–6093 (2014).

[22]T. A. W. Wolterink, R. Uppu, G. Ctistis, W. L. Vos, K.-J. Boller, and P. W. H. Pinkse, "Programmable two-photon quantum interference in 10^3 channels in opaque scattering media," Phys. Rev. A **93**, 053817 (2016).
[23]Y. Peng, Y. Qiao, T. Xiang, and X. Chen, "Manipulation of the spontaneous parametric down-conversion process in space and frequency domains via wavefront shaping," Opt. Lett. **43**, 3985–3988 (2018).
[24]H. Defienne, M. Reichert, and J. W. Fleischer, "Adaptive quantum optics with spatially entangled photon pairs," Phys. Rev. Lett. **121**, 233601 (2018).
[25]O. Lib, G. Hasson, and Y. Bromberg, "Real-time shaping of entangled photons by classical control and feedback," Sci. Adv. **6**, eabb6298 (2020).
[26]H. Cao, T. Čižmár, S. Turtaev, T. Tyc, and S. Rotter, "Controlling light propagation in multimode fibers for imaging, spectroscopy and beyond," Adv. Opt. Photon. **15**, 524–612 (2023).
[27]S. M. Popoff, G. Lerosey, R. Carminati, M. Fink, A. C. Boccara, and S. Gigan, "Measuring the transmission matrix in optics: An approach to the study and control of light propagation in disordered media," Phys. Rev. Lett. **104**, 100601 (2010).
[28]I. M. Vellekoop and A. Mosk, "Focusing coherent light through opaque strongly scattering media," Opt. Lett. **32**, 2309–2311 (2007).
[29]M. W. Matthès, Y. Bromberg, J. de Rosny, and S. M. Popoff, "Learning and avoiding disorder in multimode fibers," Phys. Rev. X **11**, 021060 (2021).
[30]S. Resisi, Y. Viernik, S. M. Popoff, and Y. Bromberg, "Wavefront shaping in multimode fibers by transmission matrix engineering," APL Photonics **5**, 036103 (2020).
[31]Z. Finkelstein, K. Sulimany, S. Resisi, and Y. Bromberg, "Spectral shaping in a multimode fiber by all-fiber modulation," APL Photonics **8**, 036110 (2022).
[32]T. Qiu, H. Cao, K. Liu, E. Lendaro, F. Wang, and S. You, "Spatiotemporal control of nonlinear effects in multimode fibers for two-octave high-peak-power femtosecond tunable source," arXiv:2306.05244 (2023).
[33]H. Cao, S.-C. Gao, C. Zhang, J. Wang, D.-Y. He, B.-H. Liu, Z.-W. Zhou, Y.-J. Chen, Z.-H. Li, S.-Y. Yu *et al.*, "Distribution of high-dimensional orbital angular momentum entanglement over a 1 km few-mode fiber," Optica **7**, 232–237 (2020).
[34]F. Steinlechner, P. Trojek, M. Jofre, H. Weier, D. Perez, T. Jennewein, R. Ursin, J. Rarity, M. W. Mitchell, J. P. Torres *et al.*, "A high-brightness source of polarization-entangled photons optimized for applications in free space," Opt. Express **20**, 9640–9649 (2012).
[35]R. Bedington, J. M. Arrazola, and A. Ling, "Progress in satellite quantum key distribution," npj Quantum Inf. **3**, 30 (2017).
[36]S.-K. Liao, W.-Q. Cai, W.-Y. Liu, L. Zhang, Y. Li, J.-G. Ren, J. Yin, Q. Shen, Y. Cao, Z.-P. Li *et al.*, "Satellite-to-ground quantum key distribution," Nature **549**, 43–47 (2017).
[37]K. Sulimany and Y. Bromberg, "All-fiber source and sorter for multimode correlated photons," npj Quantum Inf. **8**, 4 (2022).
[38]K. Garay-Palmett, D. B. Kim, Y. Zhang, F. A. Domínguez-Serna, V. O. Lorenz, and A. B. U'Ren, "Fiber-based photon-pair generation: Tutorial," J. Opt. Soc. Am. B **40**, 469–490 (2023).
[39]S. Goel, S. Leedumrongwatthanakun, N. H. Valencia, W. McCutcheon, C. Conti, P. W. H. Pinkse, and M. Malik, "Inverse-design of high-dimensional quantum optical circuits in a complex medium," arXiv:2204.00578 [quant-ph] (2022).
[40]J.-F. Morizur, L. Nicholls, P. Jian, S. Armstrong, N. Treps, B. Hage, M. Hsu, W. Bowen, J. Janousek, and H.-A. Bachor, "Programmable unitary spatial mode manipulation," J. Opt. Soc. Am. A **27**, 2524–2531 (2010).
[41]G. Labroille, B. Denolle, P. Jian, P. Genevaux, N. Treps, and J.-F. Morizur, "Efficient and mode selective spatial mode multiplexer based on multi-plane light conversion," Opt. Express **22**, 15599–15607 (2014).
[42]N. K. Fontaine, R. Ryf, H. Chen, D. T. Neilson, K. Kim, and J. Carpenter, "Laguerre-Gaussian mode sorter," Nat. Commun. **10**, 1865 (2019).
[43]U. G. Būtaitė, H. Kupianskyi, T. Čižmár, and D. B. Phillips, "How to build the 'optical inverse' of a multimode fibre," Intell. Comput. **2022**, 9816026.
[44]F. Brandt, M. Hiekkamäki, F. Bouchard, M. Huber, and R. Fickler, "High-dimensional quantum gates using full-field spatial modes of photons," Optica **7**, 98–107 (2020).
[45]M. Hiekkamäki and R. Fickler, "High-dimensional two-photon interference effects in spatial modes," Phys. Rev. Lett. **126**, 123601 (2021).
[46]O. Lib, K. Sulimany, and Y. Bromberg, "Processing entangled photons in high dimensions with a programmable light converter," Phys. Rev. Appl. **18**, 014063 (2022).
[47]D. Zheng, Y. Li, E. Chen, B. Li, D. Kong, W. Li, and J. Wu, "Free-space to few-mode-fiber coupling under atmospheric turbulence," Opt. Express **24**, 18739–18744 (2016).
[48]R. Shekel, O. Lib, A. Sardas, and Y. Bromberg, "Shaping entangled photons through emulated turbulent atmosphere," OSA Continuum **4**, 2339–2350 (2021).
[49]M. Ghalaii and S. Pirandola, "Quantum communications in a moderate-to-strong turbulent space," Commun. Phys. **5**, 38 (2022).
[50]S. P. Walborn, C. Monken, S. Pádua, and P. Souto Ribeiro, "Spatial correlations in parametric down-conversion," Phys. Rep. **495**, 87–139 (2010).